RSC Advances

PAPER

View Article Online
View Journal | View Issue

Cite this: *RSC Adv.*, 2017, **7**, 41282

Structure and photoluminescence properties of novel $Sr_6Ca_4(PO_4)_6F_2$:Re (Re = Eu^{2+}, Mn^{2+}) phosphors with energy transfer for white-emitting LEDs

Hongwei Xu, Lili Wang, Dan Qu, Zhiyun Si and Jinsheng Shi *

Received 19th June 2017
Accepted 16th August 2017

DOI: 10.1039/c7ra06817d

rsc.li/rsc-advances

A series of $Sr_6Ca_4(PO_4)_6F_2$:Eu^{2+},Mn^{2+} phosphors were synthesized through traditional solid state reaction. The structural and spectroscopic properties of the series samples along with the energy transfer from Eu^{2+} to Mn^{2+} ions have been investigated in detail. Under excitation at 295 or 365 nm, Eu^{2+} singly doped phosphors exhibit a broad emission band centered at 450 nm. When Eu^{2+} and Mn^{2+} were co-doped in $Sr_6Ca_4(PO_4)_6F_2$, a broad blue emission band peaking at 450 nm and an orange emission band at 570 nm appeared simultaneously upon ultraviolet (365 nm) excitation, which result from the 4f–5d transition of Eu^{2+} ions and the $^4T_1$–$^6A_1$ transition of Mn^{2+} ions, respectively. By controlling the doping concentration of Mn^{2+} ions, a series of tunable luminescent colors including white light are obtained with a wide band emission and a correlated color temperature of 6662 K. The possible energy transfer mechanism was proposed to be dipole–quadrupole, with regard to the analysis of photoluminescence spectra and decay curves experimental results of the series samples. The critical distance between the Eu^{2+} and Mn^{2+} ions has been calculated by both the concentration quenching method (11.53 Å) and the spectral overlap method (9.43 Å). Overall, this research indicated that the prepared samples may be potentially applied in white-light-emitting diodes under UV-pumping.

1 Introduction

As a next-generation light source, white-light-emitting diodes (w-LEDs) have gained tremendous attention because of their high color rendering, eco-friendliness, and high brightness characteristics compared to traditional fluorescent light sources.[1–6] At present, most of the commercially phosphor-converted LEDs involve a blue emitting (In,Ga)N chip with a $(Y,Gd)_3Al_5O_{12}$:Ce^{3+} phosphor. Meanwhile due to the lack of the red emission spectra, these phosphors suffer from low color rendering index and high correlated color temperature. In order to overcome these major drawbacks, an effective method is to obtain a phosphor which is a blend of blue, green, and red tricolor phosphors (RGB phosphors), which is radiated by ultraviolet (300–400 nm) light.[7–10] Using this method, a kind of w-LEDs with excellent color points can be realized. However, these phosphors exhibit low efficiencies in blue emission due to re-absorption by the other phosphors. Therefore, developing a kind of single-phase white-emitting phosphor consisting of an activator and a sensitizer with the same host is indispensable.[11–15]

One approach to realize a single phase white emitting phosphor is to co-doped Eu^{2+} and Mn^{2+} ions.[16–18] The Mn^{2+} ions doped into a sample show a broad band emission, which was assigned from the $^4T_1 \rightarrow {}^6A_1$ transition. However, electrons of the 3d shell are strongly influenced by the effect of site symmetry and crystal field strength, and Mn^{2+} emission band changes from green (week crystal field of the tetrahedrally coordinated Mn^{2+}) to red (strong crystal field of the octahedrally coordinated Mn^{2+}) region.[19–21] Additionally, owing to the forbidden d–d transitions of Mn^{2+}, the absorption and emission energy of Mn^{2+} are relatively weak. As a kind of an efficient sensitizer, Eu^{2+} can transfer energy to Mn^{2+} in many hosts. The broad emission bands covering from blue to red spectral range in Eu^{2+}/Mn^{2+} co-doped host lattices complement each other to obtain white light because of additive color mixing. Therefore, the process of the Eu^{2+} to Mn^{2+} energy transfer has been found in many systems and the corresponding mechanism has been investigated for a long time.[22–24] Earlier reports on Eu^{2+}–Mn^{2+} co-doped phosphors that realize white light emission include $Mg_2Al_4Si_5O_{18}$, $Ba_{1.3}Ca_{0.7}SiO_4$, $BaCa_2Si_3O_9$, and $NaScSi_2O_6$, *etc.*, on account of their stabilization of ionic charge, low price, and excellent thermal stability in comparison with other phosphors.[25–28] Besides, phosphate-based phosphors with multi-sites structure have attracted much attention and reported continuously, such as $Na_{2.5}Y_{0.5}Mg_7(PO_4)_6$:$Eu^{2+}$,$Tb^{3+}$,$Mn^{2+}$,[24] $Ca_9Ce(PO_4)_7$:Eu^{2+},Mn^{2+}.[29] Moreover, because of fluorine atom exhibits strongest attractive electron ability and has the largest

Department of Chemistry and Pharmaceutical Science, Qingdao Agricultural University, Qingdao 266109, People's Republic of China. E-mail: jsshiqn@aliyun.com

electronegative, phosphors which contain fluorine atoms usually show good luminescence properties and good stability. For instance, $Ca_9Mg(PO_4)_6F_2$:Eu^{2+},Mn^{2+} phosphor[16] and $Sr_5(PO_4)_4F$:Eu^{2+},Mn^{2+} phosphor,[30] *etc.* These phosphors display excellent properties and promising value in lighting applications when built into activator ions.

In this work, a series of blue to orange phosphors $Sr_6Ca_4(PO_4)_6F_2$:Eu^{2+},Mn^{2+} phosphors (SCPF:Eu^{2+},Mn^{2+}) irradiated by UV excitation, which were prepared by conventional solid state routine. The structural characteristics, luminescence behaviors of excitation and emission spectra, and luminescence quenching properties were investigated. In comparison with $Sr_5(PO_4)_3F$:Eu^{2+},Mn^{2+} phosphors, the multi-Sr^{2+}/Ca^{2+} sites in SCPF host make it possible to provide different crystal environment to Eu^{2+}/Mn^{2+} ions and give rise to about 10 nm spectral red-shift of Mn^{2+}, which is more suitable for w-LEDs upon n-UV chip excitation. While in $Ca_5(PO_4)_3F$:Eu^{2+},Mn^{2+} phosphors, similar emission behaviors can be obtained upon n-UV excitation, but only near white-light-emitting can be obtained.[31] This present work developed a new single phase, color-tunable Eu^{2+}/Mn^{2+}-doped silicate phosphor and white-light-emitting can be realized in SCPF:Eu^{2+},Mn^{2+} phosphors with the suitable color temperature value of 6662 K upon 365 nm excitation, which will match well with n-UV LEDs. In addition, all of results obtained from the experimental data and theoretical calculation are thoroughly and systematically and it can be beneficial to understand the mechanism of Eu/Mn co-doped phosphors.

2 Synthesis and characterization

2.1 Sample synthesis

The designed phosphors with a composition of (SCPF):$x$$Eu^{2+}$ (x = 0–0.06) and (SCPF):0.02Eu^{2+},$y$$Mn^{2+}$ (x = 0–0.8) powers were prepared through a high temperature solid state reaction. Power samples of $SrCO_3$ (A.R.), $CaCO_3$ (A.R.), CaF_2 (A.R.), $NH_4H_2(PO_4)_2$ (A.R.), $MnCO_2$ (A.R.), and Eu_2O_3 (99.99%) were used as the precursor materials and mixed them thoroughly for 3 h using a ball mill to obtain homogeneous samples. Afterwards, the raw materials were transferred to alumina crucibles, with subsequently sintering at 1250 °C for 4 h in reducing atmosphere, and then the as-prepared samples were cooled down to normal room temperature. Finally, all the phosphors were ground once again for further analysis.

2.2 Characterization and computational details

The structure and phase purity of as-prepared samples were analyzed by using powder X-ray diffraction (XRD) and XRD patterns are performed on D8 Focus diffractometer (Bruker) in the range from 10° to 80°, with graphite monochromatized CuKα radiation (λ = 0.15405 nm). The room temperature excitation spectra (PLE) and emission spectra (PL) were measured using a Hitachi F-4600 fluorescence spectrophotometer, which was equipped with a 150 W xenon lamp as the excitation source. Decay curves were measured on a spectrophotometer (FLS920) equipped with both a xenon lamp (450 W) and a 450 nm pulsed laser as the lighting source. UV-Vis diffuse reflectance spectra (DRS) were carried out with a UV-Vis spectrophotometer (TU-901) using $BaSO_4$ as reference. The quantum yields (QY) of the samples were measured with an integrating sphere and a FLS 920 fluorescence spectrophotometer. The temperature dependence of PL spectra was measured by using the FS-2 system and the temperature ranging from 303 K to 463 K was controlled using a homemade temperature controlled system.

To investigate the electronic structures of pure SCPF, the crystals' optimization was performed in the CASTEP program using the generalized gradient approximation (GGA) under the Perdew–Burke–Ernzerhof (PBE) formulation. During the geometry optimization, the atomic positions were optimized. The kinetic cutoff energy was 480 eV, and a K-point sampling scheme of a 5 × 5 × 5 Monkhorst–Pack grid was used. The convergence tolerance for geometry optimization was 5.0 × 10^{-6} eV per atom, the maximal ionic Hellmann–Feynman force was 1.0 × 10^{-2} eV Å^{-1}, the stress tensor was 2.0 × 10^{-2} GPa and the maximal displacement being within 5.0 × 10^{-4} Å.

3 Results and discussion

3.1 Phase and structure

Fig. 1 shows the standard data for SCPF (JCPDS#72-2399) and as-prepared samples of SCPF:0.02Eu^{2+},$y$$Mn^{2+}$ (a–e) with different Mn^{2+} content. All diffraction peaks of the XRD pattern were coincided well with that of the standard data of SCPF and the series samples can be indexed as the pure phase, which indicated that different doping concentration does not result in any other phase.

SCPF crystallizes in a hexagonal structure with space group $P6_3$(173) and three kinds of sites exist in per unit cell. The dimensions of the unit cell are $a = b$ = 9.6300 Å, c = 7.2200 Å, and V = 579.86 Å^3. A suitable viewing direction from the c axis is shown in Fig. 2(a). From the c-direction, the basic structural feature of the SCPF crystal includes CaO_6, SrO_8, and Ca/SrO_5F polyhedra are depicted. The polyhedral of Ca^{2+} and Sr^{2+} is exhibited individually in Fig. 2(b), which is consisting of the

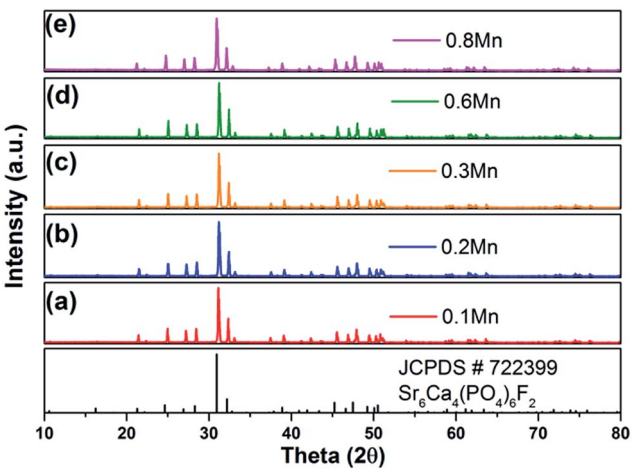

Fig. 1 XRD patterns of as-prepared SCPF:0.02Eu^{2+},$y$$Mn^{2+}$ (y = 0.1–0.8) samples and the standard data for SCPF (JCPDS#72-2399).

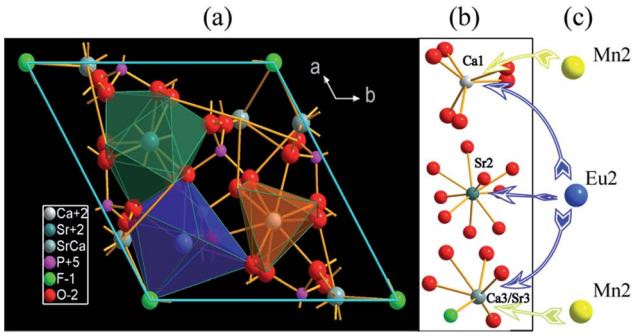

Fig. 2 Crystal structure of SCPF in a hexagonal system with space group $P6_3$(173).

Table 1 Cations in the lattice: coordination numbers (CN) and radii

Ion	P^{5+}	Ca^{2+}		Sr^{2+}		Eu^{2+}		Mn^{2+}	
CN	4	6		9		6		9	
Radii (Å)	0.38	1.18	1.26	1.18	1.30	1.17	0.83	No	

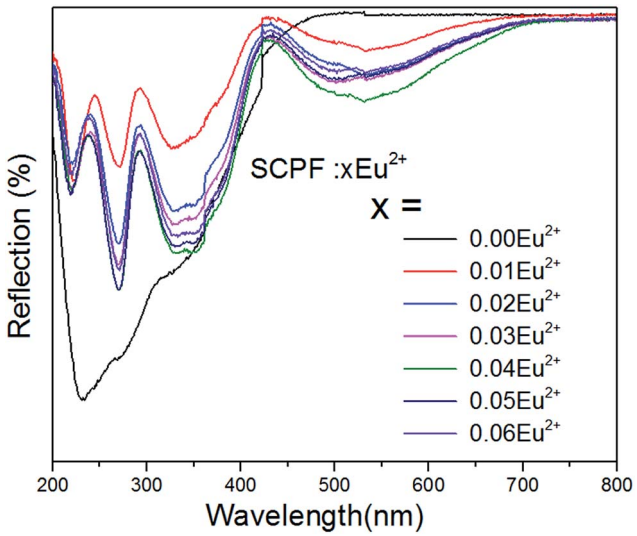

Fig. 4 Reflection spectra of SCPF:xEu^{2+} accompanying with different contents of Eu^{2+} (0–0.06), respectively.

regular octahedron of Ca1, the dodecahedron of Sr2, and the distorted octahedron of Ca3/Sr3. Based on the consideration of the ionic radius, charge and coordination, when the substitution occurs, Eu^{2+} ions prefer to occupy all the sites of Ca/Sr. Nevertheless, it worth noting that Mn^{2+} is likely to substitute Ca1 and Ca3/Sr3 sites, due to the limitation of the coordination number and the corresponding data is shown in Table 1.

The calculated atomic band structure, and total density of states (TDOS), as well as partial density of states (PDOS) for SCPF are shown in Fig. 3. The direct band gap of SCPF is about 5.182 eV from the top of the valence band (VB) to the bottom of the conduction band (CB) at the G point. The density of states of SCPF was calculated and shown in Fig. 3(b), which is beneficial to understand the composition of the energy band. It can be observed that the valence band is dominated by O 2p states and the conduction band of SCPF is composed of Sr 5s and Sr 3d states. Additionally, the partial density of states of P and F states contributes to a small extent to the valence/conduction band. With such a large band gap, the SCPF host may provide a suitable band gap for Eu^{2+}, which the energy level of the $4f^6 5d \rightarrow 4f^7$ transition has small influence on the CB and VB.[32]

3.2 Spectroscopy properties

3.2.1 Diffuse spectra of SCPF:xEu^{2+} (x = 0–0.06). The absorption of the host lattice derives from the state electrons were excited from VB to CB. Fig. 4 shows reflection spectra of the SCPF host and SCPF:xEu^{2+} (x = 0–0.06) phosphors. The host shows an obvious reflection from 200 to 800 nm. Notably, when the Eu^{2+} dopants were introduced at 1%, it can clearly be observed that a sharply enhanced broad reflection band arranging from 200 to 420 nm and a weak declined broad reflection band from 420 nm to 700 nm appeared. With further increasing concentration of Eu^{2+}, the refractive index of the series samples decrease continuously from x = 0.01 to 0.04, which was attributed to the $4f^7$–$4f^6 5d^1$ absorption of Eu^{2+}. However, once the Eu^{2+} content is more than 4%, the index of refraction of Eu^{2+} becomes strengthened.

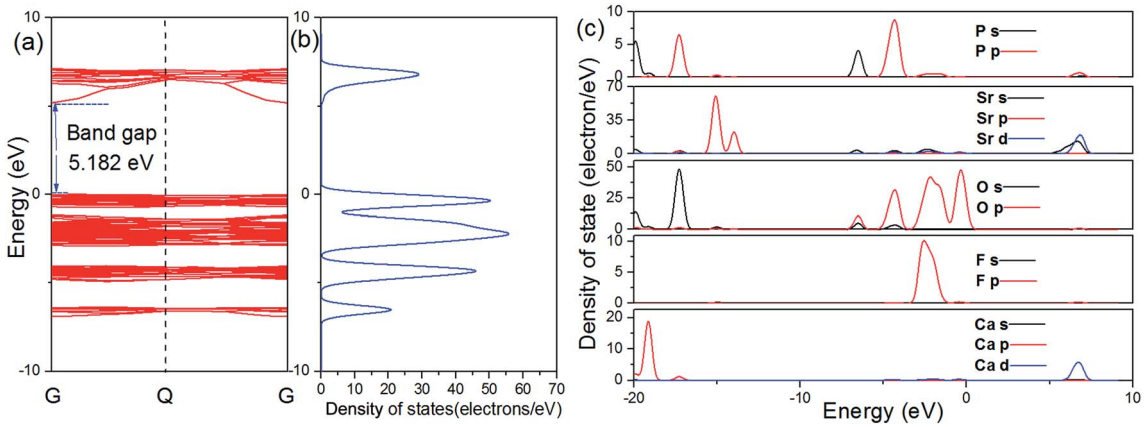

Fig. 3 Band structure (a), total density of states (b) and partial density of states of SCPF (c).

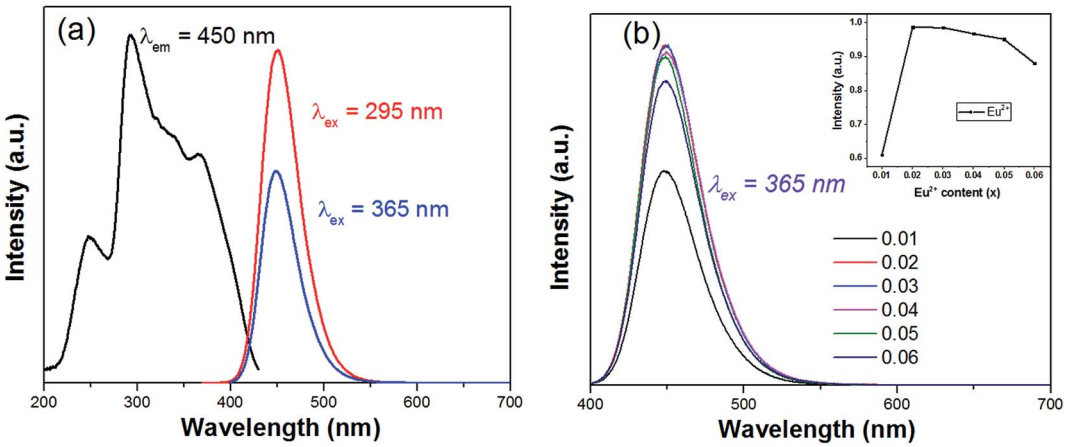

Fig. 5 (a) PLE/PL spectra of SCPF:0.02Eu^{2+}; (b) emission spectra of different Eu^{2+} contents under 365 nm excitation.

3.2.2 PL spectra and energy transfer process of SCPF:Eu^{2+} and SCPF:Eu^{2+},Mn^{2+}. Fig. 5(a) displays the PL/PLE spectra of SCPF:0.02Eu^{2+} phosphor. It can be seen that the PLE shows a broad band, which is due to the $4f^7$–$4f^65d^1$ transition of Eu^{2+} ions. Upon irradiation at 295 or 365 nm, the emission spectra of SCPF:0.02Eu^{2+} exhibits a broad symmetric band from 400 to 550 nm, with its emission peak at 450 nm. Fig. 5(b) shows the relative emission spectra of various Eu^{2+} concentrations excited at 365 nm. The PL intensity of Eu^{2+} increases initially with increasing its concentration until the Eu^{2+} content reaches at $x = 0.02$. However, once Eu^{2+} content is further increased, the emission intensity of Eu^{2+} decreased, which is because of the typical concentration quenching effect. Notably, even the addition of Eu^{2+} is 0.05 mol, its emission intensity is closely to that of the optimal concentration (0.02 mol) of Eu^{2+}. Herein, the critical distance between Eu^{2+} ions for concentration quenching was calculated by the following equation:[33]

$$R_c \approx 2\left[\frac{3V}{4\pi\chi_c Z}\right]^{1/3} \quad (1)$$

where V represents the volume of the unit cell, χ_c represents the critical concentration of the activator, and Z is the number of formula units. For the SCPF host, $Z = 1$, $\chi_c = 0.02$, and $V = 579.86$ Å. Thus, the calculated $R_c = 38.12$ Å. In generally, R_c is 5 Å typically belongs to the exchange interaction in a forbidden transition. Therefore, the type of energy transfer does not belong to exchange interactions but to electric multi-pole to multi-pole interactions.

In Fig. 6(a), the emission spectra and excitation spectra of SCPF:0.02Eu^{2+} are presented, while that of SCPF:0.6Mn^{2+} are shown in Fig. 9(b). The PL spectra of SCPF:0.02Eu^{2+} exhibits broad band from 400 to 520 nm peaking at 450 nm, while the corresponding excitation spectra of SCPF:0.6Mn^{2+} is composed of several sharp lines originated from the spin-forbidden transitions from $6A^1$(S) to $4T^1$(P) (319 nm), 4E(D) (343 nm), $4T^2$(D) (362 nm), ($4A^1$(G), 4E(G)) (406 nm), $4T^2$(G) (433 nm) and $4T^1$(G) (470 nm), *etc.*, which is covering the region of 300 to 500 nm. The effective spectral overlap areas of PL of Eu^{2+} and PLE of Mn^{2+} ensure the existence of the energy transfer (ET) between Eu^{2+} and Mn^{2+} (marked as yellow). Additionally, the corresponding excitation spectra of co-doped samples (Eu^{2+} and Mn^{2+}) were monitored at characteristic emission wavelengths of Eu^{2+} (450 nm) and Mn^{2+} (570 nm) are displayed in Fig. 6(c). In addition, it was clearly seen that the shape of excitation of Mn^{2+} was similar to that of Eu^{2+}, which means Mn^{2+} could be radiated more effectively under the sensitization of Eu^{2+}.

To further investigate the energy transfer between Eu^{2+} and Mn^{2+} in SCPF, the PL decay curves of the series samples are shown in Fig. 7(a). It can be seen that the decay curves of SCPF:0.02Eu^{2+},yMn^{2+} ($y = 0.1$–0.8) are well fitted with a typical double-exponential function:[34]

$$I = A_1 \exp\left(\frac{t}{-\tau_1}\right) + A_2 \exp\left(\frac{t}{-\tau_2}\right) \quad (2)$$

where I represents the emission intensity; t represents the time; A_1 and A_2 stand for constant; τ_1 and τ_2 are regarded as the short and long lifetimes for the exponential component, respectively. The lifetimes were calculated as follows:

$$\tau = \frac{A_1\tau_1^2 + A_2\tau_2^2}{A_1\tau_1 + A_2\tau_2} \quad (3)$$

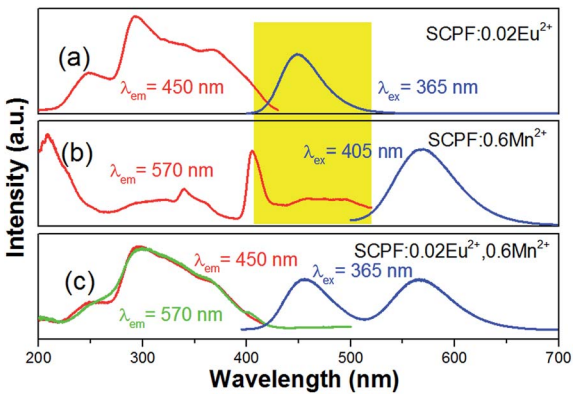

Fig. 6 (a, b) PLE/PL spectra of SCPF:0.02Eu^{2+} and 0.6Mn^{2+}, respectively; (c) PLE (monitored at 450 and 570 nm, respectively) and PL spectra of SCPF:0.02Eu^{2+},0.6Mn^{2+}.

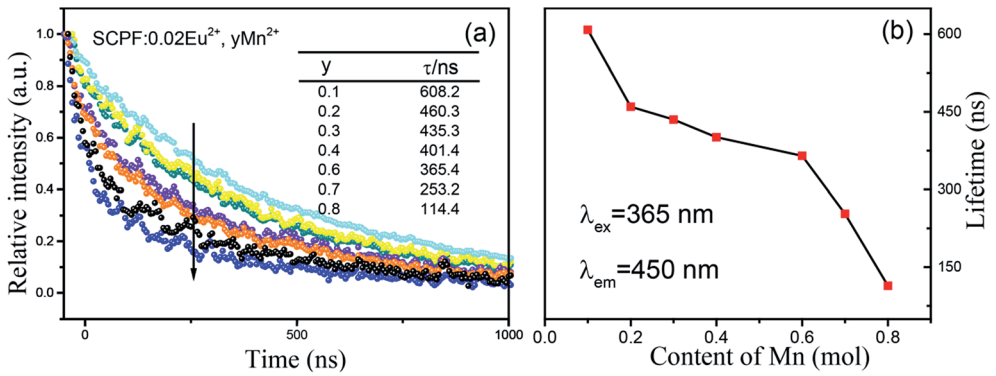

Fig. 7 Decay curves of the series SCPF samples monitored at 450 nm (a) and the corresponding lifetimes of the Mn^{2+} content plotted in (b).

Calculated decay times of Eu^{2+} for SCPF:0.02Eu^{2+},yMn^{2+} samples varied from 608.2 to 114.4 ns when monitored at 450 nm (λ_{ex} = 365 nm), showing a continuously decline. The corresponding lifetimes of the Mn^{2+} co-doped samples are plotted in Fig. 7b, which confirm the ET from Eu^{2+} to Mn^{2+}.

Fig. 8(a) shows the detailed PL spectra of the series samples. When irradiated at 365 nm, two broad bands with emission peak at 450 nm and 570 nm are detected in Eu^{2+}/Mn^{2+} co-doped samples with the quantum efficiency is 9.22%. With increasing the Mn^{2+} content, a continuous intensity decrease occurs in the emission band of Eu^{2+} (450 nm), while the emission intensity of Mn^{2+} ($4T^1(4G)$–$6A^1(6S)$) increases until the y = 0.6, and then declines slightly, which was ascribed to concentration quenching of Mn^{2+}. The inset picture of Fig. 8(a) shows the efficiency of the ET process from Eu to Mn ions, and the ET efficiency (η_T) can be estimated by the follow formula:[35]

$$\eta_T = 1 - \frac{I}{I_0} \quad (4)$$

where I and I_0 are the emission intensities for the samples in the presence and absence of Mn^{2+}, respectively. The efficiency of ET was calculated to be 87.8% when y = 0.6. Additionally, the critical distance based on the energy transfer from Eu^{2+} to Mn^{2+} (R_{Eu-Mn}) could be calculated through the concentration quenching method. The average distance R_{Eu-Mn} suggested by Blasse can be expressed as follows:[7]

$$R_{Eu-Mn} \approx 2\left[\frac{3V}{4\pi XN}\right]^{1/3} \quad (5)$$

where N is the sum number molecules in the unit cell, V is the unit cell volume, and X is the total concentration of the activator and sensitizer. For the above formula, the calculated result is 11.53 Å, which is larger than 5 Å. Therefore it is the electric multi-polar interaction instead of the exchange interaction that dominates in SCPF:0.02Eu^{2+},yMn^{2+}.

Sequentially, on the base of Dexter's energy transfer equation for multi-polar interactions, the type of energy transfer can be obtained through the spectral overlap method:[9]

$$I_0/I \propto C^{n/3} \quad (6)$$

where I_0 and I represent the luminescence intensities for samples in the absence and the presence of Mn^{2+}, respectively, and C is the total dopant concentration of Eu^{2+} and Mn^{2+}. Using eqn (6), the calculated results (n = 6, 8, 10), which correspond to the exchange interaction for dipole–dipole, dipole–quadrupole, and quadrupole–quadrupole interactions, respectively, are

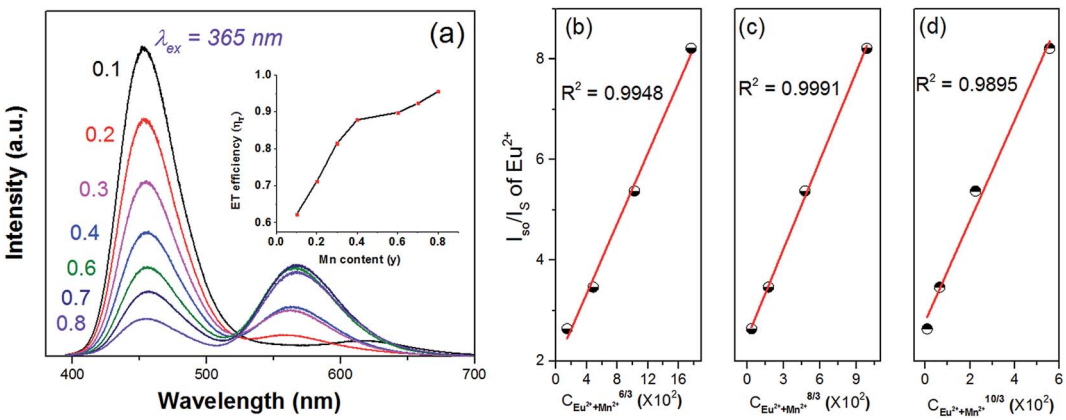

Fig. 8 (a) PL spectra of SCPF:0.02Eu^{2+},yMn^{2+} (y = 0–0.8) with the ET efficiency plotted in the inset; dependence of I_0/I (Eu^{2+}) on $C_{Eu^{2+}+Mn^{2+}}{}^{6/3}$, $C_{Eu^{2+}+Mn^{2+}}{}^{8/3}$ and $C_{Eu^{2+}+Mn^{2+}}{}^{10/3}$ and the linear fitting results (b)–(d).

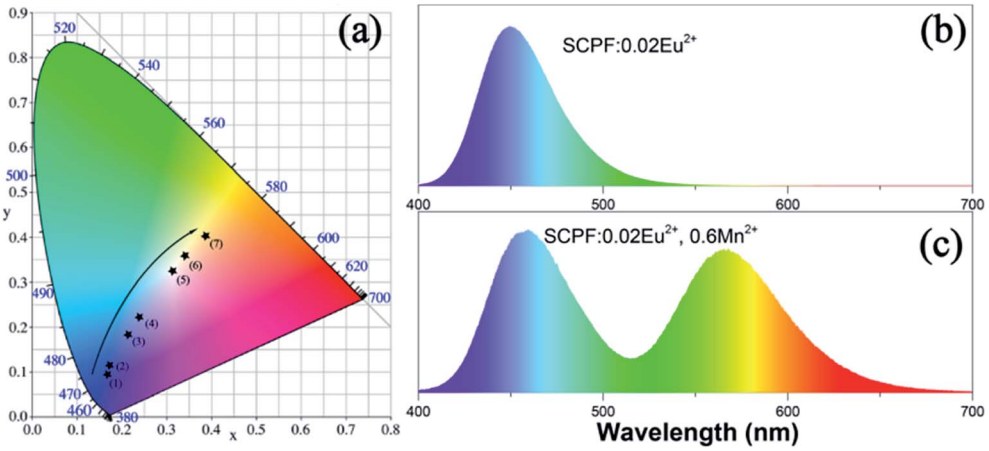

Fig. 9 (a) CIE coordinates and luminescent digital photographs of the SCPF:0.02Eu^{2+},yMn^{2+} samples under 365 nm excitation; magnifications of the emission spectra of (b) SCPF:0.02Eu^{2+} and (c) SCPF:0.02Eu^{2+},0.6Mn^{2+}.

depicted in Fig. 8(c and d). A good linear correlation is obtained when $n = 8$, indicating that the dipole–quadrupole mechanism dominated preferentially for the Eu^{2+}–Mn^{2+} energy transfer. According to the spectral overlap theory, R_{Eu-Mn} could be also calculated by the formula below:[2,36]

$$R_c^{\ 8} = 3.024 \times 10^{12} \times \lambda_{S^2} f_q \int \frac{F_s(E)F_A(E)\mathrm{d}E}{E^4} \quad (7)$$

where R_c represents the critical distance, could be calculated using the emission wavelength of Eu^{2+} (4500 Å), f_q stands for the oscillator strength of the involved absorption transition of the sensitizer (10^{-10}), $\int \frac{F_s(E)F_A(E)\mathrm{d}E}{E^4}$ is the spectral overlap between the normalized photoluminescence spectra of the Eu^{2+} emission $F_S(E)$ and the Mn^{2+} excitation $F_A(E)$. Correspondingly, the critical distance was estimated to be 9.43 Å, which is basically in good agreement with the result obtained by the quenching method described. From the above discussion (in the part of eqn (4)–(7)), it can be better understand the ET process through the ET related calculations.

The CIE coordinates of the series of samples upon 365 nm excitation, which are marked as blacked dots, are portrayed in Fig. 9(a). It can be seen that the CIE chromaticity coordinates move from blue to yellow as the amount of Mn^{2+} adds from 0 to 0.8 and the color images of SCPF:0.02Eu^{2+} and SCPF:0.02Eu^{2+},0.6Mn^{2+} are given in Fig. 9(b) and (c). The corresponding color temperature (CCT) values of the series samples are demonstrated in Table 2. With the changes of Mn^{2+} content, a warm white light emission can be obtained with a CCT of 6662 K and CIE coordinate (0.2996, 0.3118).

Table 2 Comparison of the CIE chromaticity coordinates and CCT (K) for SCPF:0.02Eu^{2+},yMn^{2+} phosphors excited at 365 nm

Sample no.	Sample composition (n)	CIE coordinates (x, y)	CCT (K)
1	$y = 0.1$	(0.1537, 0.0854)	5765
2	$y = 0.2$	(0.1633, 0.1077)	12 836
3	$y = 0.3$	(0.2026, 0.1746)	92 948 443
4	$y = 0.4$	(0.2245, 0.2096)	86 420
5	$y = 0.6$	(0.2996, 0.3118)	6662
6	$y = 0.7$	(0.3334, 0.3503)	5160
7	$y = 0.8$	(0.3803, 0.3956)	4065

4 Conclusions

In summary, a series of single-component color tunable SCPF:Eu^{2+},Mn^{2+} phosphors were synthesized through high temperature solid state reaction. The obtained phosphors of SCPF:Eu^{2+},Mn^{2+} have broad excitation bands ranging from 200 to 400 nm which match the available UV chips. The emission spectra consists of two emission bands (centered at 450 and 570 nm, respectively) by precisely controlling the ratio of Eu^{2+} to Mn^{2+}. The emission color of phosphors SCPF:Eu^{2+},Mn^{2+} can be tuned from blue to yellow and the corresponding color hue can be changed from blue (0.1537, 0.0854) to white (0.2996, 0.3118) with CCT at 6662 K. Using the concentration quenching method and the spectral overlap method, the critical distance R_{Eu-Mn} was calculated to be 11.53 Å and 9.43 Å, respectively. The energy transfer mechanism from the Eu^{2+} to Mn^{2+} ions has been demonstrated to be resonant type *via* dipole–quadrupole interaction. The investigation results indicate that the SCPF:0.02Eu^{2+},0.6Mn^{2+} phosphor might be a white-emitting phosphor for UV-excited WLEDs.

Conflicts of interest

There are no conflicts to declare.

References

1 G. Li, Y. Zhang, D. Geng, M. Shang, C. Peng, Z. Cheng and J. Lin, *ACS Appl. Mater. Interfaces*, 2012, **4**, 296–305.
2 H. Zhou, Y. Jin, M. Jiang, Q. Wang and X. Jiang, *Dalton Trans.*, 2015, **44**, 1102–1109.
3 H. Liu, Y. Luo, Z. Mao, L. Liao and Z. Xia, *J. Phys. Chem. C*, 2014, **2**, 1619.

4 Y. Liu, C. Zhang, Z. Cheng, Z. Zhou, J. Jiang and H. Jiang, *Inorg. Chem.*, 2016, **55**, 8628–8635.
5 Y. Zhu, L. Huang, R. Zou, J. Zhang, J. Yu, M. Wu, J. Wang and Q. Su, *J. Mater. Chem. C*, 2016, **4**, 5690–5695.
6 Y. Huang and H. J. Seo, *Mater. Lett.*, 2015, **156**, 86–89.
7 M. Jiao, Y. Jia, W. Lu, W. Lv, Q. Zhao, B. Shao and H. You, *Dalton Trans.*, 2014, **43**, 3202–3209.
8 X. Y. Liu, H. Guo, S. Ye, M. Y. Peng and Q. Y. Zhang, *J. Mater. Chem. C*, 2015, **3**, 5183–5191.
9 M. Shang, G. Li, X. Kang, D. Yang, D. Geng and J. Lin, *ACS Appl. Mater. Interfaces*, 2011, **3**, 2738–2746.
10 R. Shi, G. Liu, H. Liang, Y. Huang, Y. Tao and J. Zhang, *Inorg. Chem.*, 2016, **55**, 7777–7786.
11 Y. Cao, J. Ding, X. Ding, X. Wang and Y. Wang, *J. Mater. Chem. C*, 2017, **5**, 1184–1194.
12 M. Jiao, Y. Jia, W. Lü, W. Lv, Q. Zhao, B. Shao and H. You, *J. Mater. Chem. C*, 2014, **2**, 90–97.
13 F. Kang, Y. Zhang and M. Peng, *Inorg. Chem.*, 2015, **54**, 1462–1473.
14 Y. Liu, G. Liu, J. Wang, X. Dong and W. Yu, *Inorg. Chem.*, 2014, **53**, 11457–11466.
15 H. Zhu, Z. Xia, H. Liu, R. Mi and Z. Hui, *Mater. Res. Bull.*, 2013, **48**, 3513–3517.
16 K. Li, D. Geng, M. Shang, Y. Zhang, H. Lian and J. Lin, *J. Phys. Chem. C*, 2014, **118**, 11026–11034.
17 W. R. Liu, C. H. Huang, C. W. Yeh, J. C. Tsai, Y. C. Chiu, Y. T. Yeh and R. S. Liu, *Inorg. Chem.*, 2012, **51**, 9636–9641.
18 J. Ding, Q. Wu, Y. Li, Q. Long, C. Wang and Y. Wang, *Dalton Trans.*, 2015, **44**, 9630–9636.
19 H. Wang, L. Wu, H. Yi, B. Wang, L. Wu, Y. Gu and Y. Zhang, *Dalton Trans.*, 2015, **44**, 1427–1434.
20 L. Wu, B. Wang, Y. Zhang, L. Li, H. R. Wang, H. Yi, Y. F. Kong and J. J. Xu, *Dalton Trans.*, 2014, **43**, 13845–13851.
21 J. Cheng, P. Li, Z. Wang, Y. Sun, Q. Bai, Z. Li, M. Tian, C. Wang and Z. Yang, *J. Mater. Chem. C*, 2017, **5**, 127–133.
22 Y. Sun, P. Li, Z. Wang, J. Cheng, Z. Li, C. Wang, M. Tian and Z. Yang, *J. Phys. Chem. C*, 2016, **120**(36), 20254–20266.
23 X. Chen, P. Dai, X. Zhang, C. Li, S. Lu, X. Wang, Y. Jia and Y. Liu, *Inorg. Chem.*, 2014, **53**, 3441–3448.
24 Y. Xu, X. Li, W. Feng, W. Li and K. Zhang, *Dalton Trans.*, 2016, **45**, 3983–3991.
25 J. Chen, Y. Liu, M. Fang and Z. Huang, *Inorg. Chem.*, 2014, **53**, 11396–11403.
26 W. Lv, M. Jiao, Q. Zhao, B. Shao, W. Lu and H. You, *Inorg. Chem.*, 2014, **53**, 11007–11014.
27 M. Muller and T. Justel, *Dalton Trans.*, 2015, **44**, 10368–10376.
28 Z. Xia, Y. Zhang, M. S. Molokeev and V. V. Atuchin, *J. Phys. Chem. C*, 2013, **117**, 20847–20854.
29 C. Wang, P. Li, Z. Wang, Y. Sun, J. Cheng, Z. Li, M. Tian and Z. Yang, *Phys. Chem. Chem. Phys.*, 2016, **18**, 28661–28673.
30 Y. Feng, J. Huang, L. Liu, J. Liu and X. Yu, *Dalton Trans.*, 2015, **44**, 15006–15013.
31 T. Wanjun and Z. Fen, *Eur. J. Inorg. Chem.*, 2014, **2014**, 3387–3392.
32 N. Zhang, C. Guo, J. Zheng, X. Su and J. Zhao, *J. Phys. Chem. C*, 2014, **2**, 3988.
33 Z. Xia and R.-S. Liu, *J. Phys. Chem. C*, 2012, **116**, 15604–15609.
34 X. Zhang, L. Zhou, Q. Pang, J. Shi and M. Gong, *J. Phys. Chem. C*, 2014, **118**, 7591–7598.
35 T. Li, P. Li, Z. Wang, S. Xu, Q. Bai and Z. Yang, *Dalton Trans.*, 2015, **44**, 16840–16846.
36 K. Li, H. Lian, M. Shang and J. Lin, *Dalton Trans.*, 2015, **44**, 20542–20550.